Biochimica et Biophysica Acta 1842 (2014) 981–991

Contents lists available at ScienceDirect

Biochimica et Biophysica Acta

journal homepage: www.elsevier.com/locate/bbadis

Live-cell FRET imaging reveals clustering of the prion protein at the cell surface induced by infectious prions

Evandro Tavares [a], Joana A. Macedo [a], Pedro M.R. Paulo [b], Catarina Tavares [a], Carlos Lopes [a], Eduardo P. Melo [a,b,*]

[a] Centre for Molecular and Structural Biomedicine, Institute for Biotechnology and Bioengineering, Universidade do Algarve, Campus de Gambelas, 8005-139 Faro, Portugal
[b] Centro de Química Estrutural, Instituto Superior Técnico, Universidade Técnica de Lisboa, Av. Rovisco Pais 1, 1049-001 Lisboa, Portugal

ARTICLE INFO

Article history:
Received 28 August 2013
Received in revised form 14 January 2014
Accepted 4 February 2014
Available online 12 February 2014

Keywords:
Prion protein
Live-cell FRET imaging
CFP-YFP
m-turquoise2
FLIM
Prion propagation

ABSTRACT

Prion diseases are associated to the conversion of the prion protein into a misfolded pathological isoform. The mechanism of propagation of protein misfolding by protein templating remains largely unknown. Neuroblastoma cells were transfected with constructs of the prion protein fused to both CFP-GPI-anchored and to YFP-GPI-anchored and directed to its cell membrane location. Live-cell FRET imaging between the prion protein fused to CFP or YFP was measured giving consistent values of 10 ± 2%. This result was confirmed by fluorescence lifetime imaging microscopy and indicates intermolecular interactions between neighbor prion proteins. In particular, considering that a maximum FRET efficiency of 17 ± 2% was determined from a positive control consisting of a fusion CFP-YFP-GPI-anchored. A stable cell clone expressing the two fusions containing the prion protein was also selected to minimize cell-to-cell variability. In both, stable and transiently transfected cells, the FRET efficiency consistently increased in the presence of infectious prions — from 4 ± 1% to 7 ± 1% in the stable clone and from 10 ± 2% to 16 ± 1% in transiently transfected cells. These results clearly reflect an increased clustering of the prion protein on the membrane in the presence of infectious prions, which was not observed in negative control using constructs without the prion protein and upon addition of non-infected brain. Our data corroborates the recent view that the primary site for prion conversion is the cell membrane. Since our fluorescent cell clone is not susceptible to propagate infectivity, we hypothesize that the initial event of prion infectivity might be the clustering of the GPI-anchored prion protein.

1. Introduction

Prions, a class of proteinaceous infectious self-reproducing agents discovered by S. Prusiner, cause fatal neurodegenerative diseases due to misfolding and aggregation of the prion protein. Also termed transmissible spongiform encephalopathies (TSEs), these diseases occur when an abnormal isoform of the prion protein named PrP^{Sc} acts as a transmissible agent being able to induce the conversion of endogenous cellular prion protein (PrP^{C}) into new PrP^{Sc} molecules which then form aggregates. The infectious characteristic of prion diseases imposes threat to public health as shown by the outbreak of mad cow disease (BSE) in the 80s. The appearance of this novel disease in cattle, its source of infection likely to be related to feed and especially its most probable transmissibility to humans by consumption of BSE-contaminated beef products [1] has stimulated investigation on prion diseases. Moreover, the mechanism of propagation of protein misfolding by corruptive protein templating thought to be exclusive of prion diseases has now been proven to occur in other proteophaties such as Alzheimer, Parkinson and Huntington diseases conferring renewed interest to the study of prion diseases [2–4]. Increasingly efforts to solve key aspects of prion diseases have been undertaken but several questions still require definite insight such as the cell biology of prion conversion and the role of the prion protein in other neurodegenerative diseases, namely as receptor for Aβ oligomers [5], or the proteolytic cleavage of PrP^{C} impact on prion diseases [6]. The infectivity mechanism of prion diseases requires protein interaction between PrP^{Sc} and the host PrP^{C}, which is a glycoprotein anchored to the cell membrane through a glycophosphatidylinositol (GPI) anchor. The nature of the PrP^{Sc} entity is still under scrutiny and recent reports point to a dynamic collection of two distinct populations of particles [7]. Enhancement of resistance to proteolysis of PrP^{Sc} reduces its infectivity by decreasing frangibility pointing to a key role of PrP^{Sc} oligomers on infectivity [8]. It seems that rates of transmissibility and disease progression are governed by the selection of progressively less stable, faster replicating PrP^{Sc} conformers. The membrane location of PrP^{C} and especially its GPI-anchor seem to be key for prion conversion and pathogenesis [9–12]. One of the aspects that need deeper insight is certainly the characterization of the initial event in prion conversion and infectivity: (i) How do cells respond to extracellular prion aggregates? (ii) What is the initial step and where is the primary site of prion conversion? Recently, it was shown that prion infectivity is extremely rapid and the plasma

* Corresponding author. Tel. +351 289244436; fax +351 289818419.
E-mail address: emelo@ualg.pt (E.P. Melo).

http://dx.doi.org/10.1016/j.bbadis.2014.02.002
0925-4439/

membrane is the primary site for prion conversion [13]. Imaging FRET (fluorescence resonance energy transfer) has been increasingly used to examine the membrane organization of GPI-anchored proteins [14,15]. FRET measurements have the high sensitivity of fluorescence measurements and are sensitive to near-Angstrom biological relevant distances thus being widely used to study biomolecular interactions in cells [16]. The cyan and yellow fluorescent protein (CFP and YFP, respectively) pair has been commonly used to measure FRET in cells due to their excitation and emission properties, suitable Förster distance and easy photobleaching of YFP [17]. Using a novel cell system, expressing fusions between the prion protein and the CFP and YFP attached to the cell membrane through a GPI anchor, we have carried out imaging FRET measurements to characterize the interaction of infectious prions with cells. Imaging FRET can be performed in several ways including donor lifetimes [18], acceptor photobleaching [19], acceptor photoactivation [20] and variations on sensitized acceptor fluorescence also called sensitized emission [21]. Acceptor photobleaching FRET on fixed cells was first measured to characterize intermolecular FRET on this novel cell system. Then, sensitized-emission FRET was chosen to perform live-cell measurements, as the alternative based on acceptor photobleaching causes phototoxicity and it is prone to errors resulting from mobility of the donor and acceptor during scan time [22]. Using live-cell sensitized emission FRET from CFP to YFP both fused to PrP, this work shows that exogenous infectious prions promote clustering of the prion protein attached to the cell membrane as the initial step of interaction with cells.

2. Material and methods

2.1. DNA constructs

2.1.1. Site-directed mutagenesis of the mouse ORF of PrP to generate the epitope to the mAb 3F4

The ORF of mouse PrP was mutagenized targeting the residues L108M and V111M to generate the specific epitope for the mAb 3F4. The L108M mutation was first obtained with the primers 5′-cca aaa acc atg aag cat gtg gca ggg-3′ (forward) and 5′-ccc tgc cac atg ctt cat gtt ggt ttt tgg-3′ (reverse). The V111M mutation was then generated using the template with the L108M mutation and the primers 5′-cca aca tga agc ata tgg cag ggg ctg cgg-3′ (forward) and 5′-ccg cag ccc ctg cca tat gct tca tgt tgg-3′ (reverse).

2.1.2. Generation of PrP-FP-GPI constructs targeted to the plasma membrane

The sequences of YFP and CFP were ligated to the PrP sequence that codes for the GPI-anchor preceded by 15 bp from mature PrP, to assure that cleavage and GPI-anchor are processed correctly. This ligation was performed first by amplification of the fluorescence protein sequences from the plasmids pEYFP and pECFP with the primers 5′-ggg aga aga tcc agc atg gtg agc aag ggc-3′ (forward) and 5′-gga tct ccc gtc ctt gta cag ctc gtc-3′ (reverse) and by amplification of the sequence that codes for the GPI-anchor with the primers 5′-gac gag ctg tac aag gac ggg aga aga tcc-3′ (forward) and 5′-agt gga tcc tca tcc cac gat cag gaa-3′ (reverse). SOEing of the two previous PCR products was carried out using the primers 5′-gac gag ctg tac aag gac ggg aga aga tcc-3′ (forward) and 5′-gga tct tct ccc gtc ctt gta cag ctc gtc-3′ (reverse) [23]. The sequence that codes for FP-GPI was then amplified with the primers 5′-ttt tga att cat ggt gag caa ggg cga gga g-3′ (forward) and 5′-agt gga tcc tca tcc cac gat cag gaa-3′ (reverse). The forward and reverse primers have recognition sites for EcoRI and BamHI restriction enzymes, respectively. The ORF of PrP with L108M and V111M mutations was amplified to generate a GPI-anchorless sequence with recognition sites for the restriction enzymes HindIII and EcoRI using the primers 5′-ctt agg ctt atg gcg aac ctt ggc tac-3′ (forward) and 5′-gcc ctt gct cac cat gct gga tct tct ccc-3′ (reverse). The sequences YFP-GPI and CFP-GPI generated by SOEing and the PrP-anchorless sequence were digested with EcoRI and ligated with T4 ligase (Promega, USA). The resulting PrP-YFP-GPI and PrP-CFP-GPI sequences were then digested with HindIII and BamHI and cloned into pcDNA 5.0/Hyg and pcDNA 3.1/Zeo plasmids (Invitrogen, USA), respectively. Restriction enzymes were acquired both from Promega (USA) and Nzytech (Portugal).

2.1.3. Generation of FP-GPI constructs targeted to the plasma membrane

To generate constructs of YFP-GPI and CFP-GPI targeted to the plasma membrane (negative control) the sequences coding for PrP-YFP-GPI and PrP-CFP-GPI, in the respective plasmids, were used as template for the primers 5′-ctt aag ctt atc atg gcg aac ctt ggc tac tgg ctg ctg gcc ctc ttt gtg act atg tgg act gat gtc ggc ctc tgc aaa aag cgg cca aag cct atg gtg agc aag ggc gag-3′ (forward) and 5′-agt gga tcc tca tcc cac gat cag gaa-3′ (reverse). The forward primer contains the coding region for the peptide signal that directs the protein to the ER and anneals with the FP coding sequence. The resulting constructs YFP-GPI and CFP-GPI were cloned into the plasmids pcDNA 5.0/Hyg and pcDNA 3.1/Zeo, respectively.

2.1.4. Generation of CFP-YFP-GPI construct targeted to the plasma membrane

To generate the construct CFP-YFP-GPI targeted to the plasma membrane (positive control) the construct CFP-GPI was used as template to replace the GPI-anchor sequence by the recognition site for the restriction enzyme EcoRI using the primers 5′-ctt aag ctt atc atg gcg aac ctt ggc tac-3′ (forward) and 5′-tat aat gaa ttc ctt gta cag ctc gtc cat-3′ (reverse). The construct PrP-YFP-GPI amplified by PCR was subcloned into the pGEM plasmid (Promega, USA) and then restricted with HindIII and EcoRI to remove the PrP coding sequence. The CFP sequence, including the peptide signal targeting to the ER, was then ligated to the pGEM plasmid between HindIII and EcoRI to generate the construct CFP-YFP-GPI. This construct was then subcloned into pcDNA5.0/Hyg between HindIII and BamHI restrictions sites.

2.1.5. Generation of PrP-mtq2-GPI construct targeted to the plasma membrane

The sequence of m-turquoise2 (mtq2) from the pmtq2 vector was amplified using the primers 5′-ggg aga aga tcc agc atg gtg agc aag ggc-3′ (forward) and 5′-gga tct ccc gtc ctt gta cag ctc gtc-3′ (reverse) and digested with EcoRI and Bsp1407I (Thermo, Germany). After digestion, the resulting sequence was ligated to the pGem vector containing PrP-YFP-GPI to remove the YFP coding region. The newly formed PrP-mtq2-GPI sequence in pGem was digested with HindIII and BamHI and cloned into pcDNA 3.1/Zeo for mammalian expression.

2.1.6. Generation of mtq2-GPI constructs targeted to the plasma membrane

To generate the construct of mtq2-GPI targeted to the plasma membrane (negative control) the sequence coding for mtq2 from the pmtq2 plasmid was used as template for the primers 5′-ctt aag ctt atc atg gcg aac ctt ggc tac tgg ctg ctg gcc ctc ttt gtg act atg tgg act gat gtc ggc ctc tgc aaa aag cgg cca aag cct atg gtg agc aag ggc gag-3′ (forward) and 5′-gga tct tct ccc gtc ctt gta cag ctc gtc-3′ (reverse). The amplified sequence was digested with HindIII and Bsp1407I. The forward primer contains the coding region for the peptide signal that directs the protein to the ER and anneals with the FP coding sequence. The resulting construct was cloned into CFP-GPI-pcDNA 3.1/Zeo plasmid, digested with HindIII and Bsp1407I, to replace the coding sequence of CFP with that of mtq2.

2.1.7. Generation of mtq2-YFP-GPI construct targeted to the plasma membrane

To generate the construct mtq2-YFP-GPI targeted to the plasma membrane (positive control), the construct mtq2-GPI was used as template to replace the GPI-anchor sequence by the recognition site for the restriction enzyme EcoRI using the primers 5′-ctt aag ctt atc atg gcg aac ctt ggc tac-3′ (forward) and 5′-tat aat gaa ttc ctt gta cag ctc gtc cat-3′

(reverse). The construct PrP-YFP-GPI amplified by PCR was subcloned into the pGEM plasmid (Promega, USA) and then restricted with HindIII and EcoRI to remove the PrP coding sequence. The mtq2 sequence, including the peptide signal targeting to the ER, was then ligated to the pGEM plasmid between HindIII and EcoRI to generate the construct mtq2-YFP-GPI. To generate a positive control with a linker between mtq2 and YFP (residues GSLVPRGS), the sequence YFP-GPI was amplified using the primers 5′-ttt tga att cgg tag tct ggt gcc gcg tgg tag tat ggt gag caa ggg cga gga g-3′ (forward) and 5′-agt gga tcc tca tcc cac gat cag gaa-3′ (reverse). This fragment was subcloned between EcoRI and BamHI into the pGEM plasmid and then subcloned into pcDNA5.0/Hyg between HindIII and BamHI restrictions sites. All constructs were verified by DNA sequencing.

2.2. Cell culture and transfection

N2a-BOS, PK1 and PK1 cell knockdown for PrP [13] were cultured at 37 °C under 5% CO_2 in Optimem I supplemented with 10% FBS, 100 μg/mL streptomycin and 100 U/mL penicillin (Invitrogen, USA). Transfection of 1.5×10^5–3×10^5 N2a-BOS or PK1 cells was carried out in 35 mm culture dishes with 1 μg of the appropriate plasmid using Fugene 6 (Roche, Germany) according to the manufacturer's protocol (1 μg DNA: 3 μL transfection reagent). Double transfections were carried out at a ratio of 1:1 for the two plasmids. Transfections occurred overnight and then cells were incubated in fresh medium. After two days of transfection, stable clones of N2a-BOS cells were selected for one month upon incubation with 250 μg/mL of hygromycin and/or with 250 μg/mL of zeocin (Invitrogen, USA), for constructs cloned in pcDNA5.0/Hyg or pcDNA 3.1/Zeo, respectively. Stable clones expressing the constructs PrP-YFP-GPI and/or PrP-CFP-GPI were then selected under the microscope. For live-cell microscopy cells were cultured on glass bottom culture dishes (MatTek, USA). For cell fixation, these were treated with 3.7% paraformaldehyde for 15 min and then washed with PBS. Cells were infected with 10^{-3}, 10^{-5} and 10^{-7} dilutions of prion infected brain homogenate prepared in PBS (Rocky Mountain Laboratory prion strain – RML – kindly provided by A. Aguzzi and P. Schwarz).

2.3. Western blot

Cells were grown until confluence in 6 well plates, rinsed and resuspended in cold PBS. After centrifugation cells were lysed in RIPA buffer (25 mM Tris–HCl, pH 7.6, 150 mM NaCl, 1% NP-40, 1% sodium deoxycholate and 0.1% SDS) with freshly added 2 mM of PMSF (phenylmethylsulphonyl fluoride), 10 mM of $MgCl_2$, 50 μg/mL DNase and 1 μg/mL RNase. Total protein samples (240 μg) digested and non-digested with PNGase (2U) (Sigma, Germany) were separated in 12% SDS-PAGE electrophoresis, transferred to a nitrocellulose membrane for 1 h, blocked overnight with 4% non-fat dry milk in TBST (25 mM Tris–HCl, pH 7.4, 3 mM KCl, 140 mM NaCl and 0.05% Tween 20), incubated with 3F4 or POM1 anti-PrP mAbs for 1 h, incubated with Alexa Fluor 488 tagged goat anti-mouse Ab and imaged with a Typhoon Trio scanner (GE Healthcare, USA). Infected or healthy homogenized mouse brain – 1 μL of 20% (wt/vol) – was diluted in 30 μL of Triton-doc buffer supplemented with DNase and RNase and digested with 10 μg/mL proteinase K for 1 h at 37 °C. The reaction was stopped with the addition of 3 mM of PMSF and the samples were analyzed by western blot.

2.4. Immunocytochemistry

Neuroblastoma cells grown on glass coverslips were rinsed briefly with PBS, fixed and permeabilized with cold methanol (−20 °C) for 10 min and then washed twice with PBS, before blocking with 1% BSA in PBS for 30 min. Cells were washed three times and then incubated with the mouse anti-PrP monoclonal antibody POM1 in PBS/1% BSA, for 1 h at RT. Following three additional washes in PBS, cells were incubated with Alexa Fluor 647-labeled goat anti-mouse IgG1 secondary antibody diluted in PBS/1% BSA, for 1 h at RT in the dark. Cells were washed again in PBS, counterstained for 5 min with Hoechst 33342 (Invitrogen), rinsed with PBS and mounted on microscopy slides using Mowiol as mounting medium.

2.5. Cell treatment with phosphatidylinositol-specific phospholipase C

To release GPI-anchored proteins from the plasma membrane cells were washed with cold PBS and incubated with 1 U/mL of phosphatidylinositol-specific phospholipase C (PIPLC, Invitrogen) in PBS at 37 °C for 2 h. Fluorescence emission spectra of the incubation buffer were recorded in a Fluoromax 4 using excitation at 410 nm for CFP and at 488 nm for YFP.

2.6. Cell-infectivity assays

PK1 or the stable cell clone expressing the constructs PrP-YFP-GPI and PrP-CFP-GPI was seeded in 24-well plates and cultured until reaching 70% confluence. After 16 h, the cells were exposed to fresh medium containing a 10^{-3} dilution of RML 10% infectious brain homogenates. Non-infected brain homogenates were used as controls. Three days later the media was renewed before splitting 1:10. After 3 more splits the cells were transferred to a 6-well plate and grown until confluence. For immunoblotting detection of PrP^{Sc}, the cell cultures were rinsed with cold PBS and solubilized in RIPA buffer for 15 min at 4 °C. The lysate was clarified (11,000 *g*, 5 min) and the protein content in the supernatant was quantified using the Bradford method. Samples were digested with 1.2 μg of proteinase K per mg of protein for 45 min at 37 °C, stopped by the addition of 3 mM of PMSF and analyzed by western blot using the mAb POM1.

2.7. Microscopy

Steady-state fluorescence images were acquired with an inverted Carl Zeiss Axio Observer.Z1 mounted LSM710 confocal microscope with spectra detection (Carl Zeiss, Germany) using a 63× plan-apochromatic 1.4 NA oil immersion objective and a 25 mW argon laser. The microscope is equipped with a live cell imaging chamber with temperature and CO_2 control. CFP was excited at 458 nm and the emission was detected from 460 to 490 nm and YFP was excited at 514 nm and detection was from 530 to 600 nm. FRET channel for sensitized emission uses excitation at 458 nm and emission between 530 and 600 nm. The CFP and FRET channels were acquired simultaneously.

Measurements of fluorescence lifetime imaging microscopy (FLIM) were performed using a time-resolved fluorescence microscope (MicroTime 200, PicoQuant GmbH). A detailed description may be found elsewhere [18]. The excitation source is a pulsed diode laser emitting at 405 nm with a repetition rate of 20 MHz. Illumination and collection of light were done through a water immersion objective 60× magnification with NA of 1.2 (UPLSAPO 60XW, Olympus). The emitted fluorescence was spectrally selected by bandpass filters with transmission in the intervals 465–495 nm (donor channel, mtq2) and 528–563 nm (acceptor channel, YFP). Detection was done with single-photon counting avalanche diodes (Perkin-Elmer) and digitized by TimeHarp 200 TC-SPC PC board (PicoQuant GmbH). The instrument response function (IRF) has a FWHM around 0.8 ns and a time increment of 38 ps/channel. Typically, fluorescence lifetime image scans were performed over an area of tens of μm^2 with a resolution of 0.15 μm/pixel and an integration time of 2 ms/pixel. Decay fitting was performed by reconvolution with the IRF using a nonlinear least-squares procedure based on the Marquardt algorithm. The quality of the fits was evaluated by the usual criteria for the χ^2 parameter and by visual inspection of the weighted residuals.

2.8. FRET measurements and analysis

2.8.1. Acceptor photobleaching

For acceptor photobleaching FRET measurements on fixed cells, a region of interest (ROI) was bleached in the YFP channel using 20 interactions with 100% laser power at 514 nm. Pre- and post-bleach images were acquired in the CFP and YFP channels. Images were also acquired, for cells expressing CFP and YFP constructs only, to measure non-specific CFP bleaching and discard YFP to CFP photoconversion.

FRET efficiency was calculated according to:

$$E = \left(I_{CFP}^{post\ \ bleach} - I_{CFP}^{pre\ \ bleach}\right) / I_{CFP}^{post\ \ bleach} \quad (1)$$

where I_{CFP} is the fluorescence intensity of CFP.

2.8.2. Fluorescence lifetime imaging microscopy

FRET efficiency was calculated based on the fluorescence lifetime of the donor mtq2 in the absence (τ_D) and presence of acceptor YFP (τ_{DA}):

$$E = 1 - \tau_{DA}/\tau_D. \quad (2)$$

2.8.3. Sensitized-emission

For each experiment, cells with donor only (CFP), acceptor only (YFP) and both donor and acceptor were used to account for changes in donor and acceptor bleed-through depending on optical parameters. A set of three images of the same field was taken using CFP, YFP and FRET channel settings. A binary mask was created on the stack of the three images to select all the fluorescence at the surface of the cell, corresponding to fluorescent proteins attached to the cell membrane. Then, original images were multiplied by the binary image to keep pixel intensities unchanged at the fluorescent cell surface and convert pixel intensities to zero outside the ROI defined by the mask. After this treatment, FRET images were calculated as described below and represented in a rainbow scale using the Zen software from Carl Zeiss.

Sensitized-emission FRET index was calculated as follows:

$$FRET_i = I_{DA(DA)} - I_{DA(D)}/I_{DD(D)} * I_{DD(DA)} - I_{DA(A)}/I_{AA(A)} * I_{AA(DA)}. \quad (3)$$

This equation follows the nomenclature used by Zal and Gascoigne [24]. First and second letters as subscript refer to excitation and emission settings, respectively, D for donor and A for acceptor. Letters between parentheses refer to the presence of donor (D), acceptor (A) or donor and acceptor (DA). $I_{DA(DA)}$ is the intensity of the donor in the acceptor channel for cells with donor and acceptor — FRET channel. $I_{DD(DA)}$ and $I_{AA(DA)}$ are the intensities of the donor in the donor channel and of the acceptor in the acceptor channel, respectively, for cells with both donor and acceptor. $I_{DA(D)}/I_{DD(D)}$ is the intensity of the donor in the acceptor channel divided by the intensity of the donor in the donor channel for cells with donor only — donor bleed-through measured to be constant for specific optical parameters as expected [25]. A value of 0.30–0.41 was measured for donor bleed-through depending on the optical parameters used. $I_{DA(A)}/I_{AA(A)}$ is the intensity of the acceptor in the acceptor channel upon excitation with donor wavelength divided by the intensity of the acceptor in the acceptor channel for cells with acceptor only — direct excitation of the acceptor with donor wavelength also called acceptor bleed-through. Acceptor bleed-through was constant for each specific combination of optical parameters, ranging from 0.12 to 0.58 for the different optical parameters used in this work. Bleed-through coefficients for CFP and YFP were determined independently for each experiment and were found to be remarkably constant across a wide range of concentrations in cells [24]. The intensity of donor using acceptor excitation and emission settings ($I_{AA(D)}$) is zero as well as the intensity of the acceptor using donor excitation and emission settings ($I_{DD(A)}$).

Sensitized-emission live FRET imaging leads to a FRET index which is dependent on the fluorophore concentration and the optical parameters of the imaging system in use. Dependence on fluorophore concentration, intensity and variation of spectral bleed-through as a function of fluorophore intensity may be corrected using normalized FRET (NFRET) with the PixFRET plug-in of ImageJ [26]. However, NFRET is still a non-absolute value dependent on the optical parameters preventing quantitative evaluation, comparison and standardization of FRET imaging data. To overcome this disadvantage Zal and Gascoigne [24] have proposed a methodology to calculate FRET efficiency (E-FRET) as a quantitative measure independent of the optical parameters of the imaging system. E-FRET correlates with the degree of donor–acceptor interaction or clustering. The E-FRET was calculated using normalized FRET:

$$E\text{-}FRET = NFRET/(NFRET + G) \quad (4)$$

where $NFRET = FRET_i/SQRT(I_{DD(DA)} * I_{AA(DA)})$ and G is a correlation factor between the sensitized-emission and the concomitant drop in donor fluorescence experimentally determined according to:

$$G = \left(FRET_i - FRET_i^{post\ \ bleach}\right) / \left(I_{DD(DA)}^{post\ \ bleach} - I_{DD(DA)}^{pre\ \ bleach}\right). \quad (5)$$

The parameter G was measured on fixed cells, to prevent diffusion of fluorescent proteins into bleached regions, and a value of 1.7 ± 0.2 was obtained.

2.9. Statistical analysis

Results on plots are expressed as mean ± standard deviation (s.d). One-way analysis of variance (ANOVA) was performed to determine *p* values.

3. Results

3.1. Clone characterization

Neuroblastoma cells were transfected with constructs containing the full length mouse PrP at the N-terminal followed by a fluorescent protein and the coding region for the GPI-anchor peptide signal at the C-terminal. The full length PrP ORF includes the coding region for the peptide signal that directs the protein to the ER but not the coding region that signals anchorage to the cell membrane through the GPI group, which was placed after the fluorescent protein. To have a FRET pair two different constructs were designed, one with CFP and the other with YFP (named PrP-CFP-GPI and PrP-YFP-GPI, respectively). Using these constructs, we expected to have the prion protein attached to the cell membrane through a GPI-anchored fluorescent protein. N2a-BOS cells were transfected with one construct only or with both constructs sequentially and plasmid resistance markers were used to select a stable cell line, expressing one or two fusion proteins attached to the cell membrane. Selection of stable clones intended to minimize cell-to-cell and experiment variability due to different transfection efficiencies, variable transcriptional activity and variable cell substructure localization [27]. Stable clones were selected under the microscope and analyzed with confocal fluorescence microscopy (Fig. 1). Fluorescence from CFP and/or YFP was clearly detected at the cell membrane as expected, due to the presence of the peptide signaling the protein to the ER and the peptide signaling for GPI-anchoring. The double clone shows colocalization of the two fusions PrP-CFP-GPI and PrP-YFP-GPI, despite some spreading towards CFP or YFP channels (Fig. 1C). Fluorophore colocalization is diffraction limited and therefore gives no information on FRET relevant distances but paves the way to eventually detect FRET. Colocalization plots showing pixel spreading are assigned to partial colocalization [28]. In our study, pixel spreading may be the result of a non-homogeneous distribution of proteins in the

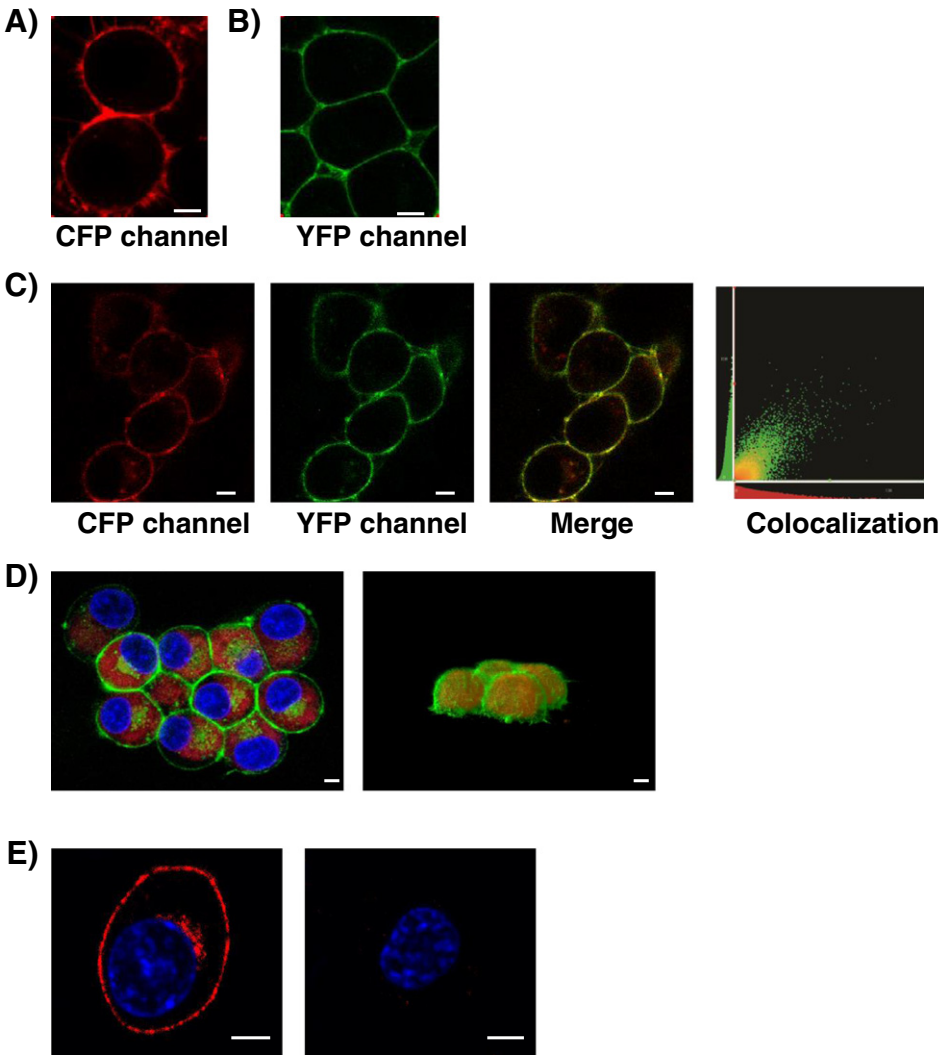

Fig. 1. Stable clones expressing the fusions PrP-CFP-GPI (A), PrP-YFP-GPI (B) and both PrP-CFP-GPI and PrP-YFP-GPI (double clone) (C). Colocalization for the fusions PrP-CFP-GPI and PrP-YFP-GPI is shown in the plot in (C) with a Pearson's coefficient of 0.75. (D) Cell substructure of the double clone showing the nuclei labeled with Hoechst 33342 in blue and the ER labeled with ER-tracker red in red (left panel). The image on the right shows a tridimensional view of the double clone, obtained after deconvolution and SFP rendering with the Huygens software (SVI, The Netherlands), to highlight the non-homogeneous distribution of fluorescent proteins on the membrane where clusters of fluorescent proteins are visible in green. The ER is shown in red. (E) Neuroblastoma cells (left panel PK1 and right panel PK1 knockdown cells) stained with mouse anti-PrP monoclonal antibody POM1 and Alexa Fluor 647-labeled goat anti-mouse IgG1 for endogenous PrP (red) and counterstained with Hoechst 33342 for nuclei (blue). Scale bars correspond to 5 μm.

membrane, with regions containing larger amounts of PrP-CFP-GPI and other regions richer in PrP-YFP-GPI. Cell substructure for the double clone was highlighted through nuclei and ER labeling using the fluorophores Hoechst 33342 and ER-tracker red (Molecular Probes), respectively (Fig. 1D, left panel). Non-homogeneous distribution of fluorescent proteins was clearly observed in the three-dimensional view of the cell membrane showing regions where clusters of fluorescent proteins occur (Fig. 1D, right panel). Whether this clustering relates to membrane microdomains such as caveolae or lipid rafts remains to be determined, namely because their size seems to be beyond the resolution of light microscopy [19]. Despite recent developments to characterize membrane microdomains, such as photonic force microscopy and single molecule microscopy, controversy still remains and size estimates for these microdomains range from 26 nm to around 700 nm [29,30]. Large microdomains substructure may result from dynamic assemblies of individual rafts [29,31]. Nevertheless, protein clustering on membrane microdomains has been detected using FRET measurements to near-Angstrom sub-diffraction resolution [19,32,33]. Membrane microdomains which form in the exoplasmic leaflet of cellular membranes can selectively incorporate protein and thereby result in protein–protein and protein–lipid interactions [31]. The pattern of fluorescence distribution in the transfected clones matches the pattern of endogenous PrP localization in neuroblastoma cells as shown in the left panel of Fig. 1E where endogenous PrP was stained with the anti-PrP monoclonal antibody POM1 [34]. The monoclonal POM1 antibody recognizes helix 1 in the globular C-terminal domain of PrP.

To certify that fusion proteins were properly processed during cell trafficking and no truncation occurred, the size of the fusion proteins was analyzed by western blot using two antibodies against PrP (Fig. 2A). The monoclonal antibody 3F4 does not react with mouse PrP as it specifically requires two Met residues at positions 108 and 111 [35]. This epitope was introduced into the fusion proteins by site-directed mutagenesis of Leu108 and Val111 to distinguish the fusion PrP-FP from the endogenous PrP^C present in N2a-BOS cells. The double clone shows three bands slightly above 50 kDa detected with both 3F4 and POM1 antibodies. These three bands have the expected size for the fusion PrP-FP (50.7 kDa) indicating no protein truncation during cell trafficking. The three bands are obviously absent in the original N2a-BOS cells and in PK1 neuroblastoma cell knockdown for PrP [13]. The presence of three bands results from different degrees of glycosylation as they shifted to a single band at smaller size after treatment with an endoglycosidase that releases N-linked oligosaccharides (PNGase).

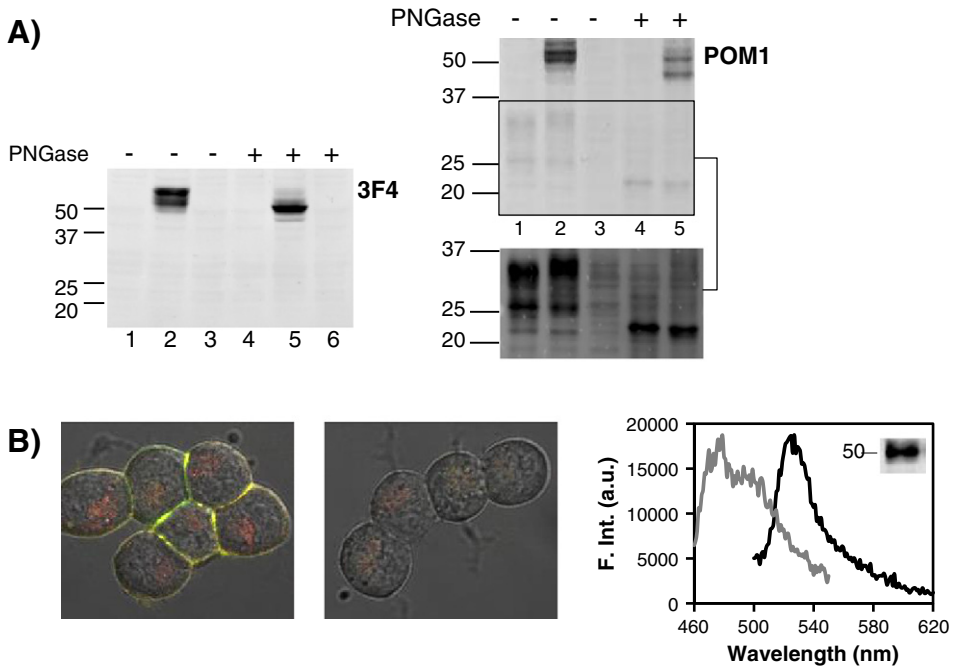

Fig. 2. (A) Western blot analysis using the monoclonal antibody 3F4 (left panel) and the monoclonal antibody POM1 (two right panels). The lower panel for POM1 shows the same region between 37 and 20 kDa, as the above but the image was acquired at higher PMT voltage to better identify the bands for endogenous PrP. N2a-BOS cells (lane 1); double clone expressing the two fusions PrP-CFP-GPI and PrP-YFP-GPI (lane 2); PK1 neuroblastoma cell knockdown for PrP (lane 3); N2a-BOS cells treated with PNGase (lane 4); double clone treated with PNGase (lane 5); PK1 neuroblastoma cell knockdown for PrP treated with PNGase (lane 6). (B) Merged fluorescence and phase contrast images comparing cells of the double clone non-treated (left image) and treated with PIPLC (right image). Note that intracellular inclusions richer in CFP (red channel) remain after treatment with phospholipase C. The plot on the right shows the fluorescence emission spectra of CFP (gray spectrum) and YFP (black spectrum) of the PBS buffer after PIPLC activity and the inset shows the western blot of the same buffer where the band of PrP-FP is detected.

The antibody POM1 recognizes both the endogenous PrP and the fusions PrP-FP-GPI (Fig. 2A, two right panels). Glycosylation of endogenous PrP was completely removed after PNGase treatment but the same treatment was not enough to completely deglycosylate the fusions PrP-FP-GPI as two bands around 50 kDa persisted. The western blot using POM1 also revealed that the expression levels of the fusion PrP-FP were considerably higher compared to the endogenous PrP. Within the same gel lane, strong bands for endogenous PrP were clearly seen only at the cost of saturating the bands for the fusion PrP (bottom panel of Fig. 2A). Endogenous PrP was absent in PK1 neuroblastoma cell knockdown for PrP used as negative control. To probe the GPI-anchor of the fusion proteins cells were incubated with PIPLC known to release PrP from the cell membrane [9]. Cell treatment with PIPLC released all the fluorescence from the cell surface, proving that PrP-FP fusions are tethered to the cell membrane through a GPI-anchor (Fig. 2B). The fluorescence emission of the supernatant was analyzed and CFP and YFP fluorescence was clearly detected as shown in the right plot of Fig. 2B. Western blot analysis of the same supernatant shows the band corresponding to the fusions PrP-FP (inset in Fig. 2B, right plot).

3.2. Acceptor photobleaching FRET measurements on fixed cells

The double clone, expressing the fusions PrP-CFP-GPI and PrP-YFP-GPI, was screened for FRET that could result from clustering of GPI-anchored proteins in membrane microdomains. Acceptor photobleaching FRET was first tried in cells transiently expressing both fusions that were fixed to avoid diffusion of new proteins into the bleached region during scanning. Fluorescence intensity of CFP increases after YFP bleaching as clearly shown in Fig. 3A. Non-bleaching of YFP in the control region leads to a very small decrease in the fluorescence of CFP and YFP, probably due to non-specific bleaching during the first scan (dashed control ROI and dashed columns in the plot of Fig. 3A). The increase in CFP fluorescence after YFP bleaching reflects a FRET efficiency that ranged from zero to around 20% for different locations on the membrane (Fig. 3B). FRET efficiency measured by acceptor photobleaching displayed a large heterogeneity of values depending on the local concentration of acceptor molecules, as previously reported [19,36]. Indeed, FRET efficiency increases when the density of acceptor molecules increases, as the excited donor has a higher probability to transfer energy to a neighboring acceptor [22]. Only if all donor and acceptor molecules are clustered in small submicron-size membrane domains FRET efficiency becomes independent of acceptor density [14,19,36]. However, it seems that only 20 to 40% of GPI-anchored proteins are organized as clusters [33]. The distribution pattern of FRET efficiency versus acceptor concentration can be used to draw conclusions on protein clustering at the cell surface [15,19,36]. Fig. 3B also shows the acceptor photobleaching FRET data for a positive control, consisting of a fusion between CFP and YFP GPI-anchored. This control reflects 100% clustering and shows that FRET is independent of acceptor concentration as expected [37]. A negative control expressing the fusions CFP-GPI and YFP-GPI (no PrP) and cells expressing both fusions containing PrP (PrP-CFP-GPI and PrP-YFP-GPI) displayed the typical saturation curve expected for partly clustered proteins. This saturable isotherm was fitted to the hyperbolic function to conclude on the degree of clustering [19]:

$$E\% = E\%_{max}\, F/(F + K)$$

where F is the fluorescence intensity of the acceptor and K is analogous to a dissociation constant providing a parameter for the degree of clustering. The fit for the negative control (no PrP) gave a K value of 8741 a.u., whereas for the cells expressing both fusions containing PrP the K value was of 7429 a.u. This indicates that the presence of PrP leads to increased clustering of GPI-anchored proteins resulting from intermolecular PrP interactions, which may induce tighter and/or long-lived protein clustering.

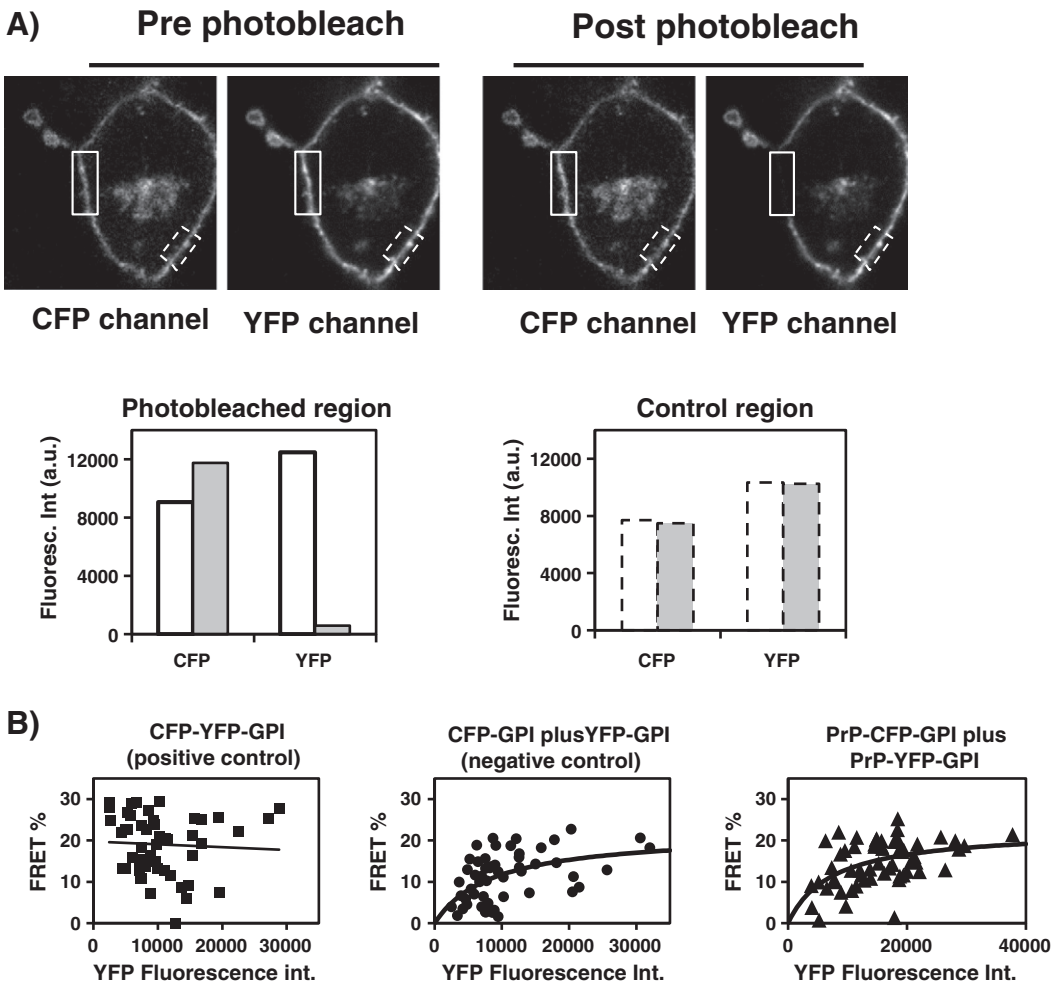

Fig. 3. Quantitative FRET images on the membrane of cells. (A) FRET images for acceptor photobleaching in fixed cells transiently transfected to express the fusions PrP-CFP-GPI and PrP-YFP-GPI. The solid rectangle shows the ROI subjected to YFP photobleaching and the dashed rectangle shows the control ROI with no photobleaching. The plots below the images show CFP and YFP fluorescence intensities for the photobleached (left plot) and the non-photobleached ROIs (right plot). White columns refer to pre-photobleaching and gray columns to post-photobleaching. The acceptor photobleaching experiment shown in the plot gave a FRET efficiency of 20% but FRET values change considerably for different locations in the membrane as shown in (B) where acceptor photobleaching FRET measurements were carried out on fixed cells, transiently transfected with: the fusion CFP-YFP-GPI — positive control (left plot); the fusions CFP-GPI and YFP-GPI — negative control (center plot) and the fusions PrP-CFP-GPI and PrP-YFP-GPI (right plot). The solid line for the positive control shows a linear equation fit to highlight the independence of FRET on acceptor intensity. Solid lines for the negative control and for cells expressing the fusions PrP-CFP-GPI and PrP-YFP-GPI show a hyperbolic function ($E\% = E\%_{max}F / (F + K)$) giving $E\%_{max}$ values of 22 and 23% and K values of 8741 and 7420 a.u., respectively.

3.3. Fluorescence lifetime imaging microscopy on fixed cells

FLIM on fixed cells was used to confirm intermolecular FRET between both fusions containing PrP. FLIM offers several advantages compared to steady-state FRET [16]. FRET efficiency is independent of the excitation intensity and of unintended photobleaching and bleed-through corrections are avoided. The fluorescence lifetime of the donor decreases when the acceptor is in close proximity (<100 Å) due to the contribution of the resonance energy transfer pathway to donor decay. However, CFP is not a suitable FRET donor for FLIM due to the complexity of its decay displaying two lifetimes and to the short average lifetime [18,37]. Therefore, CFP was replaced by the appropriate mtq2 that decays with a single-exponential, longer lifetime of 3.8–4 ns [37]. Intermolecular FRET between mtq2 and YFP was confirmed by comparing the fluorescence lifetime on membranes of cells expressing mtq2-GPI only or PrP-mtq2-GPI and PrP-YFP-GP (Fig. 4). The single lifetime of mtq2 in the absence of YFP was measured to be 3.8 ± 0.2 ns (number of ROIs ≥20) in exact concordance with the value previously reported [37] as shown in Fig. 4A and D. Orange bars in Fig. 4G show some lifetime dispersion around the average of 3.8 ns probably reflecting heterogeneous membrane environments. The decay of mtq2 in the presence of YFP remains single exponential with a lifetime of 3.5 ± 0.2 ns (Fig. 4B, E and G). The still single-exponential feature of the mtq2 decay in the presence of the acceptor YFP means that lifetime discrimination between donors transferring and non-transferring energy to YFP is not possible. The average lifetime of 3.5 ± 0.2 ns (green bars in Fig. 4G) results from a FRET efficiency of 8.1 ± 6%. This value matches the 10% FRET efficiency between CFP-GPI and YFP-GPI measured by FLIM on CHO-K1 cells [38] and is perfectly within the range of values measured in our work by acceptor photobleaching (Fig. 3B) and sensitized-emission on live cells (see data below). The lifetime of mtq2 in the positive control (fused to YFP with the linker GSLVPRGS in between) was 3.2 ± 0.2 ns (Fig. 4C, F and G) resulting from a FRET efficiency of 16 ± 5%, also perfectly within the range measured by acceptor photobleaching and sensitized emission. FLIM measurements carried out in our cell system were unable to distinguish between the population of molecules placed at FRET and non-FRET relevant distances as fluorescence decays remain single-exponential but they provide an independent prove that FRET occurs between our fluorescent proteins GPI-anchored to the cell membrane. Based on their

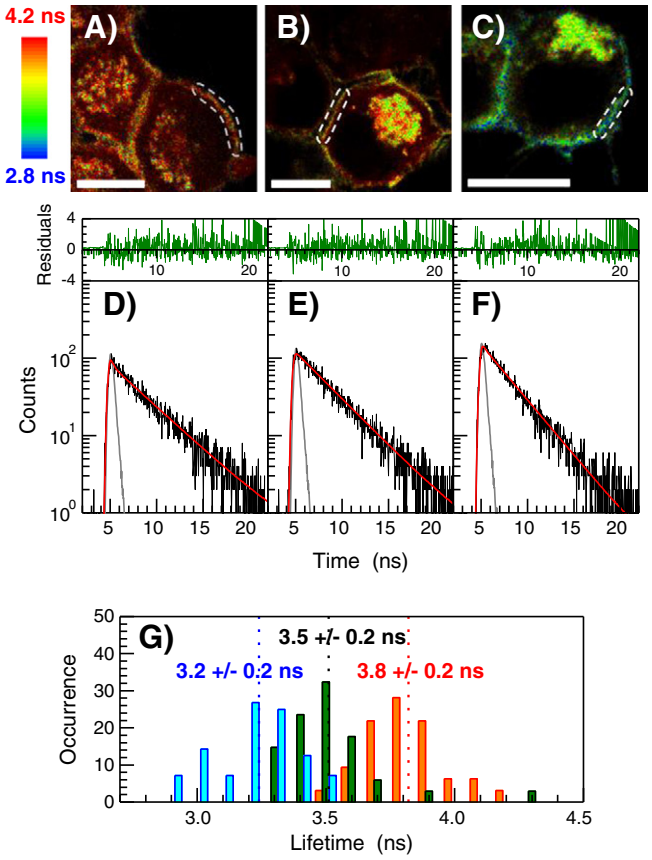

Fig. 4. FLIM images and fluorescence decays for fixed cells expressing transiently the fusion mtq2-GPI (A and D), the fusions PrP-mtq2-GPI and PrP-YFP-GPI (B and E) and the fusion mtq2-YFP-GPI used as positive control (C and F). The lifetime scale for both images is shown on the left and white bars correspond to 10 μm. Fluorescence decays shown in D, E and F were obtained from the regions of interest shown in images A, B and C as dashed white boxes. The weighed residuals from the respective single exponential fits are shown above the decays. (G) Lifetime histograms from fluorescence decays collected from ≥20 ROIs of interest over 5 image scans on cells expressing only mtq2-GPI (orange bars), expressing the two constructs PrP-mtq2-GPI and PrP-YFP-GPI (green bars) and expressing the fusion mtq2-YFP-GPI (cyan bars).

independence of concentration and bleed-through, FLIM measurements also provided an independent proof for FRET efficiencies measured by acceptor photobleaching and sensitized emission.

3.4. Live-cell sensitized emission FRET measurements

Live-cell sensitized emission FRET was then measured in the stable clone expressing both fusions, after selecting all the surface of the cell as ROI. The average absolute efficiency of FRET was calculated for all the cell membrane according to Zal and Gascoigne [24] and data is shown in Fig. 5. These E-FRET sensitized-emission values were significantly more consistent than the majority of values measured by acceptor photobleaching for cells transiently expressing both fusions because they reflect average FRET efficiency for all the cell membrane. Also, PrP expression in the stable clone was lower but more constant between cells. Live-cell sensitized emission FRET was measured for cells in the absence and presence of a 10^{-3} dilution of non-infected and prion infected brain. E-FRET values at the cell surface showed an increase in the number of green to red pixels in the presence of prion-infected brain (Fig. 5A and B). This indicates that the presence of exogenous prions promoted the clustering of the prion protein at specific locations of the cell surface leading to an increase in FRET efficiency. Heterogeneity of FRET efficiencies at the cell surface, reflected in pixels with distant scaled-colors, is expected especially in the presence of exogenous prions which should interact with specific locations in the membrane. In fact, differences in energy transfer between different cells, different ROIs or even pixels should represent different local densities of acceptor- and donor-labeled molecules within clusters, as referred above and observed in other reports [14,32]. Therefore, to clearly distinguish and quantify FRET efficiencies between cells in the absence and presence of prions, all the fluorescent surface of the cell membrane was selected as ROI and average intensities were used to calculate absolute E-FRET values (Fig. 5C). We have measured E-FRET on a significant number of cells ($12 < n < 35$) but plotted only the top 50% values. This criterion was applied equally to all situations (no brain, non-infected brain and prion-infected brain) and is justified by the fact that not all the cells are in contact with exogenous prions and PrP expression levels change from cell-to-cell, even in the stable clone. Indeed, recent work reports that up to 30% of cells in culture were infected in the presence of exogenous prions [13]. Plotting the top 50% values compares cells that may be more sensitive to increased clustering, leading to a more representative analysis of the events. Nevertheless, plotting 100% of the values measured does not change the pattern nor the conclusions taken (see Supplementary material S1). FRET efficiency increased from 3.9 to 4.5% to 7% in the presence of a 10^{-3} dilution of exogenous prions one day after infection. When 10^{-5} or 10^{-7} dilutions of prion-infected brain were used the E-FRET values obtained were 4.4 and 4.5%, respectively. The increase in FRET efficiency in the presence of a 10^{-3} dilution of prion-infected brain was statistically significant, confirming the clustering of the prion protein at the cell surface induced by prions. After three days of infection, E-FRET values increased slightly for all conditions and the E-FRET value in the presence of a 10^{-3} dilution of the prion-infected brain was still higher than in the other conditions (8.3% compared to 4.8–6.3%). Clustering of lipid-modified proteins on membranes was previously detected for GPI-anchored GFP and for fusions of CFP and YFP with short peptides containing sequences for acylation and prenylation [19,33,39]. Average FRET efficiency increased significantly to 10% in neuroblastoma live-cells transiently transfected, due to the large amounts of PrP-FP-GPI attached to the cell membrane (Fig. 5D). E-FRET sensitized-emission values increased from 10 to 11% to 16% in the presence of a 10^{-3} dilution of prion-infected brain, reflecting an increased clustering in the presence of exogenous prions as observed with the stable cell clone. This range of E-FRET values, especially the 16% measured in the presence of exogenous prions, reflects a high degree of clustering as the positive control, consisting of a fusion of CFP and YFP GPI-anchored (CFP-YFP-GPI construct), displayed 17% of FRET efficiency (Fig. 5D). To address the effect of the prion protein on protein clustering measured by live-cell sensitized emission, the negative control consisting of cells transiently transfected with the fusions CFP-GPI and YFP-GPI attached to the cell membrane was analyzed (Fig. 5D). This negative control also showed some degree of FRET due to clustering of GPI-anchored proteins on rafts, as shown above by acceptor photobleaching and reported previously for GFP-GPI using homo-FRET measurements [33]. However, E-FRET values for this negative control were slightly lower than the values measured for the fusions containing PrP, reflecting interactions between neighbor PrP molecules that may occur to increase the degree of protein clustering at the cell surface. Clustering of GPI-anchored proteins seems to be rather loose and/or transient [39] and PrP intermolecular interactions might induce tighter or long-lived protein clustering. More interestingly, the presence of exogenous prions did not increase E-FRET values for the negative control and therefore did not promote protein clustering. Protein clustering at the cell surface induced by exogenous prions only occurred for the GPI-anchored prion protein as part of the fusion protein, hence it must result from a specific interaction between infectious prions and the GPI-anchored prion protein.

3.5. Cell-infectivity assays

Cell-based infectivity assays were developed for mouse scrapie prions based on the resistance of PrP^{Sc} to PK digestion [40]. We have

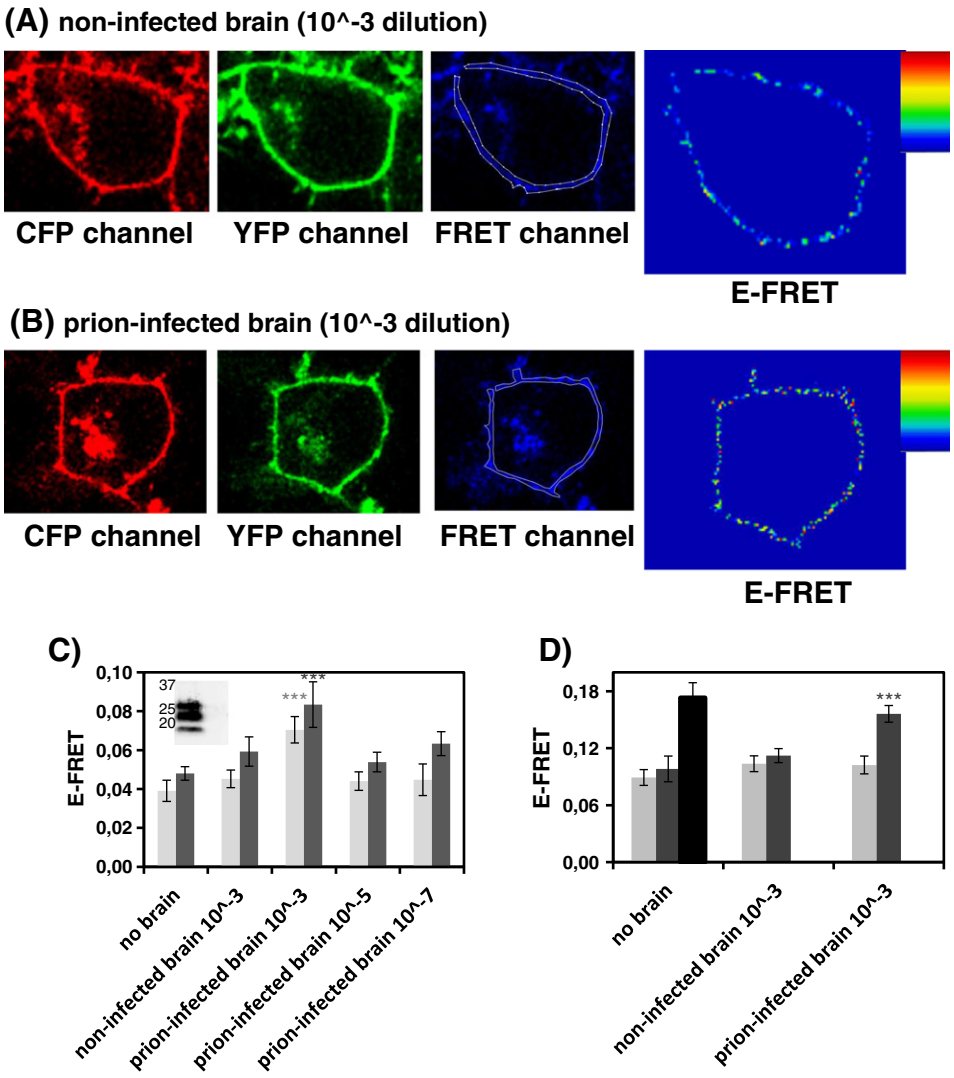

Fig. 5. Quantitative FRET images at the surface of live cells expressing the fusions PrP-CFP-GPI and PrP-YFP-GPI, CFP-GPI and YFP-GPI used as negative control and CFP-YFP-GPI only. (A) Quantitative FRET images using sensitized emission in live cells stably expressing the fusions PrP-CFP-GPI and PrP-YFP-GPI in the presence of a 10^{-3} dilution of non-infected brain. (B) Quantitative FRET images using sensitized emission in live cells stably expressing the fusions PrP-CFP-GPI and PrP-YFP-GPI in the presence of a 10^{-3} dilution of prion-infected brain. The ROI where E-FRET was calculated is shown only in the FRET channel for visual clarity. The E-FRET image is shown in a rainbow pseudocolor scale. (C) Plot with the absolute E-FRET values for the stable double clone measured in the absence of the brain, presence of a 10^{-3} dilution of non-infected brain and presence of 10^{-3}, 10^{-5} and 10^{-7} dilutions of prion-infected brain. Light gray bars refer to the stable clone one day after infection and dark gray bars refer to the stable clone three days after infection. The inset shows the western blot for the infected brain (left lane) and non-infected brain (right lane) after PK digestion. (D) Plot with the absolute E-FRET values for cells transiently transfected in the absence of the brain, presence of a 10^{-3} dilution of non-infected brain and presence of a 10^{-3} dilution of prion-infected brain. Light gray bars refer to cells transiently transfected with the constructs CFP-GPI and YFP-GPI (negative control), dark gray bars refer to cells transiently transfected with the constructs PrP-CFP-GPI and PrP-YFP-GPI and the single black bar refers to the positive control transiently transfected with the fusion CFP-YFP-GPI. The number of cells analyzed was $12 < n < 35$ but only the top 50% E-FRET values were plotted for all conditions (no brain, non-infected brain and prion-infected brain). ***The mean difference is significant at the level $p < 0.001$.

tested the susceptibility of our stable cell clone to propagate infectivity from RML mouse prions using the highly susceptible PK1 neuroblastoma cell line as positive control [13]. Fig. 6 shows that our cell clone is unable to propagate RML mouse prions at least at detectable amounts compared to the susceptible PK1 cells. The presence of the three bands of PrP^{Sc} resistant to PK was detected on infected PK1 cells only and even the endogenous PrP present in our stable cell clone has not acquired resistance to PK. The stable fluorescent cell clone selected probably originates from a non-susceptible N2a cell clone which would explain why the endogenous PrP was unable to propagate infectivity.

4. Discussion

Intermolecular FRET for GPI-membrane anchored proteins was previously detected including with FLIM measurements [33,38]. In this work, we probed intermolecular FRET between GPI-anchored fluorescent proteins fused to the prion protein. FRET was unequivocally probed by acceptor photobleaching of YFP acting as acceptor from CFP (Fig. 3) and by FLIM of the suitable mtq2 acting as donor to YFP (Fig. 4).

Live-cell intermolecular FRET was then measured for the pair PrP-CFP-GPI-anchored and PrP-YFP-GPI-anchored. Sensitized-emission was used to perform live-cell FRET in order to avoid phototoxicity due to bleaching. Using all the fluorescent surface of the cell as ROI we aimed at probing clustering of the prion protein attached to the cell membrane. The analysis of cells expressing both fusions with the prion protein compared to cells expressing CFP-GPI-anchored and YFP-GPI-anchored only (negative control with no PrP) showed that the presence of PrP increases slightly the clustering of GPI-anchored proteins (Figs. 3 and 5). Interaction between neighbor PrP molecules may promote clustering of GPI-anchored proteins. This interaction might be physiologically relevant despite the higher expression levels

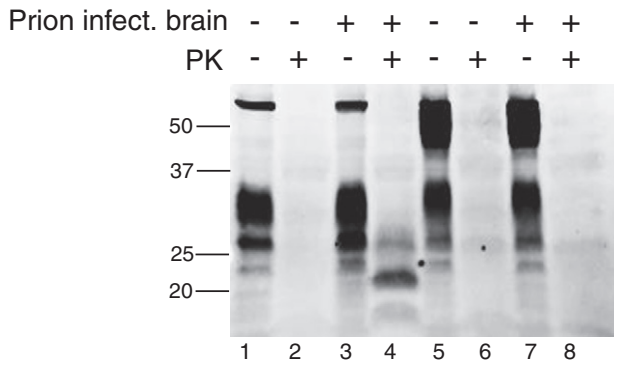

Fig. 6. Western blot analysis using the monoclonal antibody POM1. PK1 cells (lanes 1–4); double clone expressing the two fusions PrP-CFP-GPI and PrP-YFP-GPI (lanes 5–8). Note the appearance of PK resistant PrP^{Sc} detected after three splits in PK1 cells incubated with a 10^{-3} dilution of RML prion infected brain (lane 4) and its absence for the double clone (lane 8). The band appearing above 50 kDa for PK1 cells (lanes 1 and 3) is a non-specific band from the mAb POM1.

of the fusions PrP-FP-GPI compared to the endogenous PrP (Fig. 2). The prion protein was shown to dimerize in a GPI-dependent manner at the plasma membrane and dimer formation was implicated in the stress-protective activity of PrP [41]. Additionally, we have observed that our cells compared to the parental N2a-BOS cells adhere much strongly to the surface of the culture flask, indicating that our fusions containing PrP may be functional at least regarding cell adhesion (see Supplementary material S2). Stronger adhesion is certainly related to the proposed function of PrP on cell adhesion [42].

Moreover, this study shows that exogenous infectious prions promote clustering of the FP-GPI-anchored prion protein (Fig. 5). This process ought to represent the initial step of prion infectivity. Despite the observation that our stable cell line is unable to propagate infectivity as no PrP^{Sc} resistant to PK digestion is accumulated (Fig. 6), it seems tempting to establish a direct correlation between increased clustering of PrP in the presence of exogenous prions and the mechanism of prion conversion. Transgenic mice, as well as chronically infected cell cultures, expressing PrP tagged at its amino terminus with GFP were shown to support prion replication [43]. Moreover, our data corroborates the current view on the mechanism of prion infectivity. Firstly, it was shown that the plasma membrane is the primary site for prion conversion [13]. Secondly, soluble PrP^{Sc} oligomers caused synapse damage via clustering of syalylated GPI-anchors attached to PrP [10]. The sialic acid modification, which is a rare modification of mammalian GPI-anchors, seems to modify the membrane microenvironment (rafts) surrounding clustered PrP molecules resulting in aberrant activation of phospholipase A_2 and synapse damage. Using an independent live-cell biophysical approach based on FRET, we were able to support these two recent observations regarding the initial step of prion infectivity: infectious prions interact with PrP at the plasma membrane and this interaction results in an increased clustering of the GPI-anchored prion protein. These two observations help to elucidate the pathogenic cascade underlying prion diseases. One of the downstream steps that were identified recently consists in the persistent repression of protein translational rates through phosphorylation of the translational initiation factor eIF2α. This is no more than a persistent unchecked activation of the ER unfolded protein response leading to neurodegeneration [44]. The concentration of clustered molecules within a membrane plane is thought to be an important element for signaling [45] and the prion protein has been associated with several signaling molecules such as tyrosine kinase [46], protein kinase A [47] and cytoplasmic phospholipase A_2 [48]. According to the common view that individual rafts cluster together to connect raft proteins and interacting proteins into signaling complexes [45], increased PrP clustering may interfere with signaling cascades.

The prion protein is necessary for prion replication but to a large extent dispensable for the host. Therefore, screening for compounds that decrease levels of cell-surface PrP has been used to select for antiprion agents [49]. FRET measurements between antibodies labeled with donor or acceptor were used to assess PrP expression levels making the screen expensive and labor consuming. The novel cell system based on live-cell FRET measurements, established in this work, allows for direct readouts proportional to cell-surface PrP expression and it can be applied to high throughput screening assays for therapeutic approaches against prion diseases.

To conclude, confocal fluorescence imaging was carried out on neuroblastoma cells expressing fusions between the prion protein and fluorescent proteins GPI-anchored to the cell membrane to mimic the endogenous location of the prion protein. Live-cell FRET measurements indicate that increased interactions between neighbor prion protein molecules are the initial event of prion interaction with cells and may represent the initial step of prion replication and infectivity.

Supplementary data to this article can be found online at http://dx.doi.org/10.1016/j.bbadis.2014.02.002.

Acknowledgements

This work was supported by project grants PTDC/QUI-BIQ/119677/2010 and PTDC/CTM-NAN/2700/2012 (Fundação para a Ciência e Tecnologia (FCT), Portugal). Additional funding through FCT, project ref. PEst-OE/EQB/LA0023/2011 is acknowledged. E Tavares and J.A. Macedo hold a Ph.D. (SFRH/BD/48664/2008) and Post-Doctoral (SFRH/BPD/64932/2009) fellowship from FCT, respectively. Acknowledgements are due to Catarina Madeira, a former post-doctoral student, for designing the constructs to fuse PrP with FPs, to Claudia Tavares from the Light Microscopy Facility, and to Prof. Jorge Martins from the Laboratory of Physical Biochemistry at UAlg. A. Aguzzi and P. Schwarz kindly provided N2a-BOS cells and mouse prion-infected brain. A particular thanks is due to Profª. Sílvia Costa from Centro de Química Estrutural for all the support on FLIM measurements. Prof. Jorge Martins is acknowledged for fluorescence facilities.

References

[1] A. Aguzzi, C. Zhu, Five questions on prion diseases, PLoS Pathog. 8 (2012) 1–4.
[2] L.C. Walker, H. LeVine III, Corruption and spread of pathogenic proteins in neurodegenerative diseases, J. Biol. Chem. 287 (2012) 33109–33115.
[3] C. Münch, A. Bertolotti, Propagation of the prion phenomenon: beyond the seeding principle, J. Mol. Biol. 421 (2012) 491–498.
[4] S.B. Prusiner, S. B., A unifying role for prions in neurodegenerative diseases, Science 336 (2012) 1511–1513.
[5] J. Laurén, D.A. Gimbel, H.B. Nygaard, J.W. Gilbert, S.M. Strittmatter, Cellular prion protein mediates impairment of synaptic plasticity by amyloid-beta oligomers, Nature 457 (2009) 1128–1132.
[6] T. Haldiman, C. Kim, Y. Cohen, W. Chen, J. Blevins, L. Qing, M.L. Cohen, J. Langeveld, G.C. Telling, Q. Kong, J.G. Safar, Co-existence of distinct prion types enables conformational evolution of human PrP^{Sc} by competitive selection, J. Biol. Chem. 288 (2013) 29846–29861.
[7] H.C. Altmeppen, J. Prox, B. Puig, F. Dohler, C. Falker, S. Krasemann, M. Glatzel, Roles of endoproteolytic α-cleavage and shedding of the prion protein in neurodegeneration, FEBS J. (2013), http://dx.doi.org/10.1111/febs.12196.
[8] I. Margalith, C. Suter, B. Ballmer, P. Schwarz, C. Tiberi, T. Sonati, J. Falsig, S. Nyström, P. Hammarström, A. Åslund, K.P.R. Nilsson, A. Yam, E. Whitters, S. Hornemann, A. Aguzzi, Polythiophenes inhibit prion propagation by stabilizing prion protein (PrP) aggregates, J. Biol. Chem. 287 (2013) 18872–18887.
[9] M. Enari, E. Flechsig, C. Weissmann, Scrapie prion protein accumulation by scrapie-infected neuroblastoma cells abrogated by exposure to a prion protein antibody, Proc. Natl. Acad. Sci. U. S. A. 98 (2001) 9295–9299.
[10] C. Bate, A. Williams, Neurodegeneration induced by clustering of syalylated glycosylphosphatidylinositols of prion proteins, J. Biol. Chem. 287 (2012) 7935–7944.
[11] K. Kaneko, M. Vey, M. Scott, S. Pilkuhn, F.E. Cohen, S.B. Prusiner, COOH-terminal sequence of the cellular prion protein directs subcellular trafficking and controls conversion into the scrapie isoform, Proc. Natl. Acad. Sci. U. S. A. 94 (1997) 2333–2338.
[12] A. Taraboulos, M. Scott, A. Semenov, D. Avraham, L. Laszlo, S.B. Prusiner, Cholesterol depletion and modification of COOH-terminal targeting sequence of the prion protein inhibit formation of the scrapie isoform, J. Cell Biol. 129 (1995) 121–132.
[13] R. Goold, S. Rabbanian, L. Sutton, R. Andre, P. Arora, J. Moonga, A.R. Clarke, G. Schiavo, P. Jat, J. Collinge, S.J. Tabrizi, Rapid cell-surface prion protein conversion revealed using a novel cell system, Nat. Commun. 2 (2011) 281–291.

[14] A.K. Kenworthy, M. Edidin, Distribution of a glycosylphosphatidylinositol-anchored protein at the apical surface of MDCK cells examined at a resolution of <100 Å using imaging fluorescence resonance energy transfer, J. Cell Biol. 142 (1998) 69–84.
[15] A.K. Kenworthy, N. Petranova, M. Edidin, High-resolution FRET microscopy of cholera toxin B-subunit and GPI-anchored proteins in cell plasma membranes, Mol. Biol. Cell 11 (2000) 1645–1655.
[16] Y. Chen, J.D. Mills, A. Periasamy, Protein localization in living cells and tissues using FRET and FLIM, Differentiation 71 (2003) 528–541.
[17] R.M. Siegel, F.K.M. Chan, D.A. Zacharias, R. Swofford, K.L. Holmes, R.Y. Tsien, M.J. Lenardo, Measurements of molecular interactions in living cells by fluorescence resonance energy transfer between variants of the green fluorescent protein, Sci. STKE 38 (2000) pl1.
[18] C. Madeira, N. Estrela, J.A.B. Ferreira, S.M. Andrade, S.M.B. Costa, E.P. Melo, Fluorescence lifetime imaging microscopy and fluorescence resonance energy transfer from cyan to yellow fluorescent protein validates a novel method to cluster proteins on solid surfaces, J. Biomed. Opt. 14 (2009) 044035.
[19] D.A. Zacharias, J.D. Violin, A.C. Newton, R.Y. Tsien, Partitioning of lipid-modified monomeric GFPs into membrane microdomains of live cells, Science 296 (2002) 913–916.
[20] R.N. Day, M.W. Davidson, Fluorescent proteins for FRET microscopy: monitoring protein interactions in living cells, Bioessays 34 (2012) 341–350.
[21] M.W. Gordon, G. Berry, X.H. Liang, B. Levine, B. Herman, Quantitative fluorescence resonance energy transfer measurements using fluorescence microscopy, Biophys. J. 74 (1998) 2702–2713.
[22] C. Berney, G. Danuser, FRET or no FRET: a quantitative comparison, Biophys. J. 84 (2003) 3992–4010.
[23] R.M. Horton, Z. Cai, S.N. Ho, L.R. Pease, Gene splicing by overlap extension: tailor-made genes using the polymerase chain reaction, Biotechniques 8 (1990) 528–535.
[24] T. Zal, N.R.J. Gascoigne, Photobleaching-corrected FRET efficiency imaging of live cells, Biophys. J. 86 (2004) 3923–3939.
[25] T. Zal, M.A. Zal, N.R.J. Gascoigne, Inhibition of T cell receptor–coreceptor interactions by antagonist ligands visualized by live FRET imaging of the T-hybridoma immunological synapse, Immunity 16 (2002) 521–534.
[26] J.N. Feige, D. Sage, W. Wahli, B. Desvergne, L. Gelman, PixFRET, an ImageJ plug-in for FRET calculation that can accommodate variations in spectral bleed-throughs, Microsc. Res. Tech. 68 (2005) 51–58.
[27] T.C. Voss, I.A. Demarco, R.N. Day, Quantitative imaging of protein interactions in the cell nucleus, Biotechniques 38 (2005) 413–424.
[28] S. Bolte, F.P. Cordelières, A guided tour into subcellular colocalization analysis in light microscopy, J. Microsc. 224 (2006) 213–232.
[29] G.J. Schütz, G. Kada, V.Ph. Pastushenko, H. Schindler, Properties of lipid microdomains in a muscle cell membrane visualized by single molecule microscopy, EMBO J. 19 (2000) 892–901.
[30] A. Pralle, P. Keller, E.-L. Florin, K. Simons, J.K.H. Hörber, Sphingolipid–cholesterol rafts diffuse as small entities in the plasma membrane of mammalian cells, J. Cell Biol. 148 (2000) 997–1007.
[31] E. Ikonen, Roles of lipid rafts in membrane transport, Curr. Opin. Cell Biol. 13 (2001) 470–477.
[32] H. Wallrabe, M. Elangovan, A. Burchard, A. Periasamy, M. Barroso, Confocal FRET microscopy to measure clustering of ligand–receptor complexes in endocytic membranes, Biophys. J. 85 (2003) 559–571.
[33] P. Sharma, R. Varma, R.C. Sarasij, K. Gousset Ira, G. Krishnamoorthy, M. Rao, S. Mayor, Nanoscale organization of multiple GPI-anchored proteins in living cells, Cell 116 (2004) 577–589.
[34] M. Polymenidou, R. Moos, M. Scott, C. Sigurdson, Y.Z. Shi, B. Yajima, I. Hafner-Bratkovic, R. Jerala, S. Hornemann, K. Wutrich, A. Bellon, M. Vey, G. Garen, M.N.G. James, N. Kav, A. Aguzzi, The POM monoclonals: a comprehensive set of antibodies to non-overlapping prion protein epitopes, PLoS ONE 3 (2008) e3872.
[35] C. Lund, C.M. Olsen, H. Tveit, M.A. Tranulis, Characterization of the prion protein 3F4 epitope and its use as a molecular tag, J. Neurosci. Methods 165 (2007) 183–190.
[36] T. Pentcheva, M. Edidin, Clustering of peptide-loaded MHC class I molecules for endoplasmic reticulum export imaged by fluorescence resonance energy transfer, J. Immunol. 166 (2001) 6625–6632.
[37] J. Goedhart, D. von Stetten, M. Noirclerc-Savoye, M. Lelimousin, L. Joosen, M.A. Hink, L. van Weeren, T.W.J. Gadella, A. Royant, Structure-guided evolution of cyan fluorescent protein towards a quantum yield of 93%, Nat. Commun. 3 (2012) 751.
[38] S. Scolari, S. Engel, N. Krebs, A.P. Plazzo, R.F.M. De Almeida, M. Prieto, M. Velt, A. Herrmann, Lateral distribution of the transmembrane domain of Influenza vírus hemagglutinin revealed by time-resolved fluorescence imaging, J. Biol. Chem. 284 (2009) 15708–15716.
[39] D.A. De Angelis, G. Miesenböck, B.V. Zemelman, J.E. Rothman, PRIM: proximity imaging of green fluorescent protein-tagged polypeptides, Proc. Natl. Acad. Sci. U. S. A. 95 (1998) 12312–12316.
[40] P.-C. Klöhn, L. Stoltze, E. Flechsig, M. Enari, C. Weissmann, A quantitative, highly sensitive cell-based infectivity assay for mouse scrapie prions, Proc. Natl. Acad. Sci. U. S. A. 100 (2003) 11666–11671.
[41] A.S. Rambold, V. Müller, U. Ron, N. Ben-Tal, K.F. Winklhofer, J. Tatzelt, Stress-protective signalling of prion protein is corrupted by scrapie prions, EMBO J. 27 (2008) 1974–1984.
[42] E. Málaga-Trillo, G.P. Solis, Y. Schrock, C. Geiss, L. Luncz, V. Thomanetz, C.A.O. Stuermer, Regulation of embryonic cell adhesion by the prion protein, PLoS Biol. 7 (2009) e1000055.
[43] J. Bian, K.E. Nazor, R. Angers, M. Jernigan, T. Seward, A. Centers, M. Green, G.C. Telling, GFP-tagged PrP supports compromised prion replication in transgenic mice, Biochem. Biophys. Res. Commun. 340 (2006) 894–900.
[44] J.A. Moreno, H. Radford, D. Peretti, J.R. Steinert, N. Verity, M.G. Martin, M. Halliday, J. Morgan, D. Dinsdale, C.A. Ortori, D.A. Barrett, P. Tsaytler, A. Bertolotti, A.E. Willis, M. Bushell, G.R. Mallucci, Sustained translational repression by eIF2α-P mediates neurodegeneration, Nature 485 (2012) 507–511.
[45] K. Simons, D. Toomre, Lipid rafts and signal transduction, Nat. Rev. Mol. Cell Biol. 1 (2000) 31–40.
[46] S. Mouillet-Richard, M. Ermonval, C. Chebassier, J.L. Laplanche, S. Lehmann, J.M. Launay, O. Kellermann, Signal transduction through prion protein, Science 289 (2000) 1925–1928.
[47] L.B. Chiarini, A.R.O. Freitas, S.M. Zanata, R.R. Brentani, V.R. Martins, R. Linden, Cellular prion protein transduces neuroprotective signals, EMBO J. 21 (2002) 3317–3326.
[48] C. Bate, M. Tayebi, A. Williams, Phospholipase A_2 inhibitors protect against prion and Aβ mediated synapse degeneration, Mol. Neurodegener. 5 (2010) 13–24.
[49] Y.E. Karapetyan, G.F. Sferrazza, M. Zhou, G. Ottenberg, T. Spicer, P. Chase, M. Fallahi, P. Hodder, C. Weissmann, C.I. Lasmézas, Unique drug screening approach for prion diseases identifies tacrolimus and astemizole as antiprion agents, Proc. Natl. Acad. Sci. U. S. A. 110 (2013) 7044–7049.